Title

Interplay between cortical adhesion and membrane bending regulates the formation of microparticles

Journal

Soft Matter

ISSN

1744-683X

Authors

Mahapatra, Arijit

Malingen, Sage

Rangamani, Padmini

Publication Date

2026-02-01

DOI

10.1039/d5sm01237f

Soft Matter

PAPER

View Article Online
View Journal

Cite this: DOI: 10.1039/d5sm01237f

Interplay between cortical adhesion and membrane bending regulates the formation of microparticles

Arijit Mahapatra,[ac] Sage A. Malingen[ad] and Padmini Rangamani *[ab]

Received 12th December 2025,
Accepted 8th January 2026

DOI: 10.1039/d5sm01237f

rsc.li/soft-matter-journal

Cells release vesicles that serve important roles in long-range signaling and intercellular communication. These vesicles are released not just in response to stress, inflammation, injury, and chemoresistance, but also during homeostatic regulation. A particular class of vesicles called ectosomes or microparticles are released by the outward budding of the plasma membrane, a process which requires both the detachment of the membrane from the cortex and the exposure of negatively charged, curvature-inducing lipids such as phosphatidylserine from the inner leaflet to the outer leaflet. In this work, we develop a biophysical model that accounts for the interaction between these different factors. Using our model, we predict how linker properties influence outward budding of the plasma membrane and identify conditions that can promote or inhibit membrane curvature generation. These findings provide insight into the fundamental mechanisms underlying microparticle formation, elucidating the basic biology of this critical process. Further, these mechanistic insights may inspire techniques for inhibiting microparticles where they are harmful, such as chemoresistant drug efflux by tumor cells.

Introduction

Many cells in the animal body release extracellular vesicles from their cell surface under normal and stress conditions.[1–3] Circulating microparticles (MPs) are critical for cell–cell communication and are reflective of a state of inflammation in the body.[4] Conditions that introduce cell stress such as inflammation, proapoptotic conditions, and environmental stressors such as hyperbaric pressure in divers can result in increase in MP formation.[2] To avoid confusion, in this work, when we say cellular microparticles (MPs), we are referring to those vesicles that are released from the cellular plasma membrane, also referred to as ectosomes or microvesicles. Their formation is distinct from other vesicles that result from multivesicular bodies fusing with the plasma membrane and releasing their content into the extracellular space. MPs are fragments of the plasma membrane released in response to an activating stimulus such as oxidative stress, cytokines, or mechanical forces. They are also released from proapoptotic cells. MPs range in size from about 50 to 1000 nm.[5]

Microparticles were first observed to form from red blood cells in the early 1900s.[6–8] In the 1970s, a series of studies showed that MPs from normal human red blood cells could be induced by elevation of intracellular calcium, which can lead to alterations in the lipid profile of the erythrocyte membrane and release of spectrin-free vesicles.[9–11] The formation of microparticles in red blood cells is also associated with aging and maturation of these cells.[12,13] Over the years, many different cell types including platelets and endothelial cells have been known to release MPs, which have been implicated in many different physiological and pathological conditions[14–16] (Fig. 1A).

Many experimental studies have characterized the different steps in MP formation and we briefly summarize them here grouped by either membrane effects or cytoskeletal effects. One of the hallmarks of MP formation is phospholipid asymmetry in the plasma membrane (Fig. 1B). Influx of local Ca^{2+} can induce MP formation by disrupting the transporters that, in a resting state, maintain the asymmetry of the leaflets.[17–19] Phosphatidylserine (PS), a negatively charged phospholipid, which is a known marker of apoptosis, has also been found to externalize from the inner to the outer leaflet of the membrane in a host of reversible processes unrelated to cell death.[20] The timescale of PS exposure and its localization varies with the process, with a longer timescale ($\sim$1 hour) and global exposure during apoptosis and localized exposure driven by Ca^{2+} signaling on the order of 5–15 minutes[20] in non-apoptotic events. In fact, the exposure of PS on the outer leaflet is characteristic of MPs and the regions of the plasma membrane that eventually bud into MPs are shown to be rich in PS on the outer leaflet as observed by Annexin V binding.[5,17]

[a] Department of Mechanical and Aerospace Engineering, University of California San Diego, USA
[b] Department of Pharmacology, University of California San Diego, La Jolla, CA 92093-0636, USA. E-mail: prangamani@health.ucsd.edu; Tel: +1 858-534-4056
[c] Gamma Technolgies, LLC, Westmont, IL 60559, USA
[d] Department of Biology, University of Washington, USA

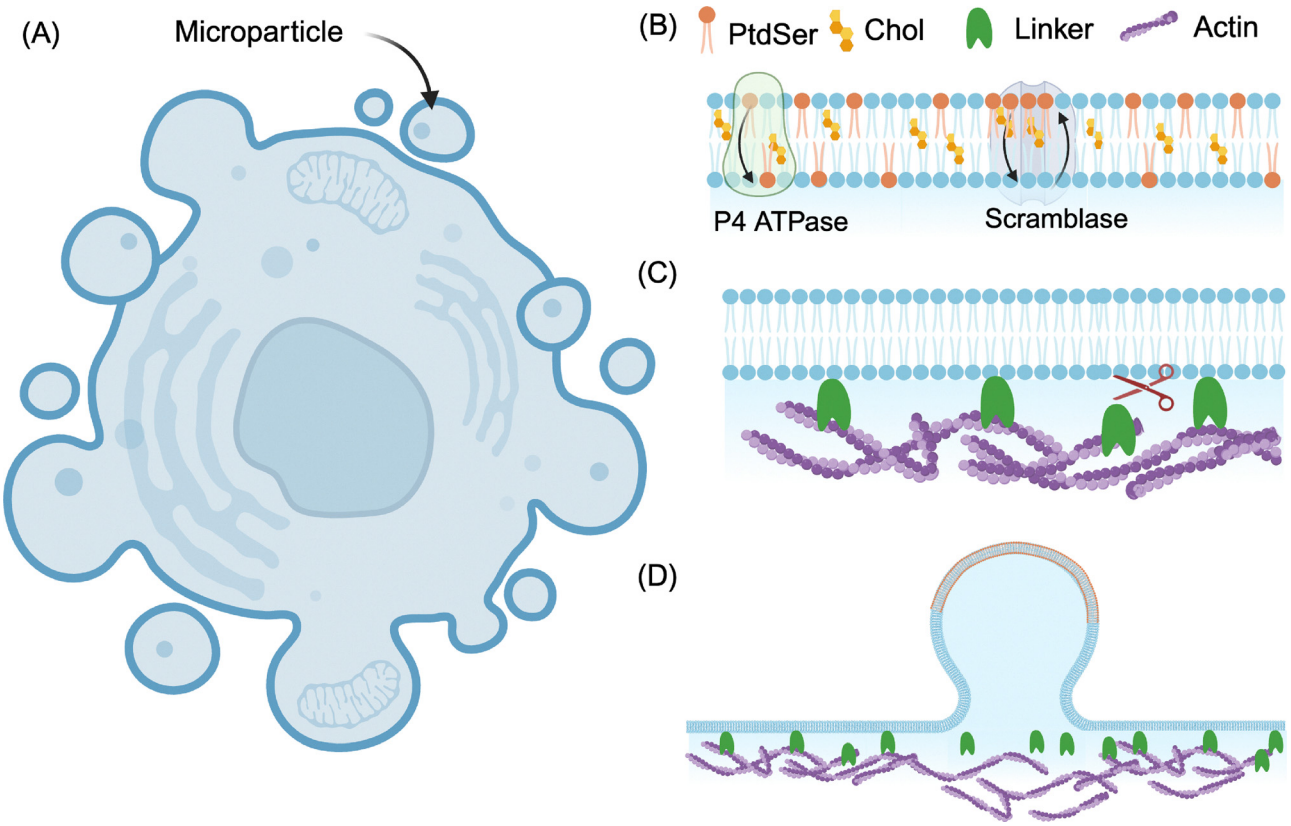

Fig. 1 Formation of microparticles on the cell surface is a biophysical process. (A) A schematic depicting microparticles being released from the plasma membrane of a cell. (B) A key initiator of microparticle formation is the exposure of phosphatidylserine (PS) on the plasma membrane, which is usually on the inner leaflet. P4ATPases are the flippases that flip the PS on the outer leaflet back to the inner leaflet and scramblases can promote lipid translocation between both leaflets. During microparticle formation, the scramblase TMEM16F translocates PS to the outer leaflet. (C) The cortical cytoskeleton is attached to the cell membrane by linkers, including those of the ezrin-radixin-moesin family. Detachment of the linkers from the membrane is a critical step for membrane deformation. (D) In this work, we model the formation of a microparticle by considering the combined role of the PS microdomain-induced curvature and detachment of the cortex by the linkers breaking. This figure was created using Biorender.com.

Significantly, it has been demonstrated that cells can adjust the preferred curvature of their membrane using PS since the negatively charged head groups of this anionic phospholipid repel one another, generating a preferred curvature.[21] The generation of lipid asymmetry on the bilayer with PS exposure on the outer leaflet has been extensively reviewed in the literature.[18,22–24]

Another important feature in MP formation is the disruption of the links between the cortical cytoskeleton and the plasma membrane (Fig. 1C). Calcium signaling can also disrupt the integration of the membrane and cortex. Ca^{2+} activates calpain, which can disrupt linkages between the membrane and the cortex.[25] Activated calpain can cleave the cortex, promoting cytoskeletal remodeling.[26] Loss of membrane-cytoskeleton integration can reduce the rigidity of the membrane,[19,27,28] in addition to reducing the adhesive force. Taken together, the delamination of the membrane from the cortex could result in a locally susceptible region along the cell membrane for outward budding. Indeed, the formation of blebs in cell membranes is accompanied by the loss of membrane cytoskeleton adhesion.[29] Recent experiments have shown that for a cell protrusion to form, actin polymerization alone is not sufficient. In fact, breakage of the actin membrane links, specifically, ezrin, is a required condition for cell protrusion – increase in actin-membrane attachment decreases protrusions while a decrease in actin-membrane attachment increases protrusions.[30] Ezrin and related proteins are also involved in MP formation,[31] suggesting that loss of membrane-cytoskeleton attachment is a critical first step in MP formation.

Thus, from a biophysical point of view, MP formation can be characterized by three main driving forces: changes in membrane composition and accompanying changes in spontaneous curvature due to PS flipping, loss of membrane-cortex attachment by breaking the adhesive bonds, and pressure-driven bleb growth (Fig. 1D). Each of these processes has been studied using mathematical models. The formation of membrane curvature due to spontaneous curvature induced by lipid-composition has been studied using the Helfrich model[32,33] and the specific role of PS has recently been incorporated into these models.[21] A biophysical model of membrane-cortex linkage examined the relationship between force, linker stiffness, and membrane curvature in the regime of small deformations.[34] In this work, we develop a combined model of membrane-cortex attachment and spontaneous curvature due to lipid asymmetry and systematically investigate the role of linker adhesion and dynamics of the

change of lipid composition in the formation of MPs. We do not focus on the role of pressure induced blebbing since it has been studied in other works.[35,36]

Specifically, we focus on the following questions: How does the kinetics of PS flipping interface with linker binding–unbinding kinetics? And how do membrane properties affect the formation of microparticles? Our model predicts that linker binding is a key determinant of MP formation. Strong linker binding can override other mechanisms of membrane deformation including PS-induced spontaneous curvature. Our simulations reveal that tuning PS-flipping kinetics through the associated enzymes, linker properties, and membrane properties give rise to interesting crosstalk for regimes of delamination of the membrane from the cortex and subsequent outward bending. These findings play a critical role in integrating myriad experimental observations in the literature and providing a unifying mechanical framework for the formation of microparticles.

Model development

In this work, the formation of microparticles is modeled as the outward bending of the membrane, away from the cytosol, in response to the accumulation of phosphatidylserine (PS) on the outer leaflet and as a result of the detachment of the cortical linkers from the plasma membrane. The biophysical model contains three main modules. Module 1: describes how the mechanics of how the membrane bends in response to the clustering of PS, which is assumed to induce spontaneous curvature; Module 2: incorporates the force-dependent kinetics of cortical linker binding and unbinding to capture the effects of the ezrin-radixin-moesin (ERM) family of proteins; and Module 3: includes the kinetics of PS flipping onto the outer leaflet of the membrane due to the activity of the specific enzymes known as scramblases. The three modules are coupled through the impact of linker adhesion and PS aggregation on the membrane energy and the spontaneous curvature induced by PS flipping, which ultimately leads to membrane bending (Fig. 1D).

Module 1: membrane energy

We assume that the membrane is a two-dimensional fluid interface with negligible thickness and can have in-plane viscous flow.[37,38] We also assume that the membrane is inextensible in the plane and elastic in out-of-plane bending with uniform bending rigidity.[39] As before,[40] we consider the total membrane energy to include the translational entropy of PS lipids on the outer leaflet, aggregation of the PS lipids, which can lead to domain formation, and bending of the membrane due to the spontaneous curvature induced by the PS lipids. We define η as the area fraction of PS on the outer leaflet and $[\mathrm{PS}]_{\mathrm{sat}}$ as the saturation density of PS on the outer leaflet. The membrane may bend in response to lipid asymmetry, which is encoded in the spontaneous curvature, $C = \ell[\mathrm{PS}]$. We assume the spontaneous curvature is directly proportional to the density of PS on the outer leaflet as before.[21,41] The membrane may also bend in response to an externally applied force, f_{pull} (see SI for normal and tangential stress balances). The inextensibility of the membrane is captured by the tension, λ.[37–39,42] The Helfrich Hamiltonian[33] describes the free energy density (W) of the membrane deformation modified with the work done by the external force density (f), such as cortex force on the membrane. The modified free energy density reads as

$$\begin{aligned} W \;=\; & \underbrace{k_{\mathrm{B}}T[\mathrm{PS}]_{\mathrm{sat}}[\eta\log\eta+(1-\eta)\log(1-\eta)]}_{\text{translational entropy of PS}} \\ & + \underbrace{\frac{\gamma[\mathrm{PS}]_{\mathrm{sat}}}{2}\eta(1-\eta)+\frac{\gamma}{4}|\nabla\eta|^2+}_{\text{aggregation of PS}} \underbrace{\kappa\left(H-\ell[\mathrm{PS}]_{\mathrm{sat}}\eta\right)^2+\bar{\kappa}K}_{\text{bending due to spontaneous curvature}} \\ & + \underbrace{\lambda}_{\text{membane tension}} - \underbrace{f\cdot\mathbf{z}}_{\text{work done by external forces}} \end{aligned} \tag{1}$$

In the above equation, H is the mean curvature of the membrane, K is the Gaussian Curvature, κ is the bending modulus, $\bar{\kappa}$ is the Gaussian modulus, and $\mathbf{z}$ is the vertical displacement of the membrane. $k_{\mathrm{B}}T$ represents the thermal energy scale. γ represents the interaction energy between PS lipids and is used to capture the following experimental observations. Even though PS is a negatively charged lipid[43,44] needref, it is known to form enriched domains on the plasma membrane under different conditions, primarily in the presence of cations like calcium or magnesium[45–48] or due to interactions with cholesterol.[49] Such aggregation also depends on the lipid phase with the liquid-ordered phase being more preferable than the liquid disordered phase.[49] We use the Cahn–Hilliard framework as before[40] to capture such molecular complexities of PS interactions in our model.

Module 2: adhesion and detachment of linkers

In order for the membrane to bend outward to form microparticles, studies have shown that the detachment of the lipid bilayer from the actin cortex is an important first step.[30,50] The attachment of the membrane to the actin cortex is through linker proteins, and we model these linkers similar to the model proposed in ref. 34, 51 and 52. The kinetics of linker binding and unbinding are given by

$$\frac{\mathrm{d}\phi_{\mathrm{lin}}}{\mathrm{d}t} = k_{\mathrm{on}}[1-\phi_{\mathrm{lin}}] - k_{\mathrm{off}}(z)\phi_{\mathrm{lin}}, \tag{2}$$

where ϕ_{lin} is the fraction of bound linkers, k_{on} is the association rate, and k_{off} is the dissociation rate of the linkers to the membrane. The rate of dissociation, k_{off}, increases with the magnitude of the force exerted by the cortex through Bell's law[34,53] and is given by $k_{\mathrm{off}} = k_{\mathrm{off}}^0 e^{\frac{\hat{F}\delta}{k_{\mathrm{B}}T}}$. Here, δ is the bond length of the linkers and $\hat{F} = k_{\mathrm{lin}}z$, where k_{lin} is the stiffness of the linker springs. The membrane shape and linker kinetics are coupled through the vertical distance z. We note that while some models have proposed a coupling between bound linker density and spontaneous curvature,[54,55] experiments showed that ezrin did not induce any membrane curvature.[56] Therefore, we did not couple linker density to spontaneous curvature in our model. To ensure that the linkers will detach when stretched beyond a certain

length, we implemented a cutoff distance (d_0) for the unbinding of the linker. If the membrane displacement from cortex layer z is greater than d_0, all linkers at that location will unbind from the membrane. Therefore, at every point on the membrane,

$$\phi_{\text{lin}}(t) = \begin{cases} \int^{t} (k_{\text{on}}(1-\phi_{\text{lin}}(\tau)) - k_{\text{off}}\phi_{\text{lin}}(\tau))\mathrm{d}\tau, & \text{if } z < d_0, \\ 0, & \text{if } z > d_0. \end{cases} \tag{3}$$

Here τ is the variable for integration over time. This is implemented numerically in the timestepping algorithm by comparing z at every location against d_0, which is fixed at 25 nm.[56–59] When z exceeds the threshold, we set ϕ_{lin} to zero along the membrane.

Module 3: phospatidylserine flipping and generation of spontaneous curvature

PS is a negatively charged lipid and is usually present on the inner leaflet of the plasma membrane.[43,44] The density of PS on the outer leaflet of the membrane is regulated by lipid translocation between leaflets due to the activity of scramblases such as TMEM16F[18,60–62] and lipid flipping from the outer leaflet to the inner leaflet due the P4ATPases (Fig. 1B).[23,63–66] Furthermore, TMEM16F appears to induce membrane thinning, promoting a curvature-dependent feedback loop[61] and P4ATPases also appear to function in a curvature-dependent manner.[66] Thus, MP formation is associated with accumulation of PS in the outer leaflet. We modeled the asymmetry introduced by these lipids using a spontaneous curvature, denoted by C, which is localized to the region of lipid asymmetry.[64] As in previous works,[21,64,67] we assume that the spontaneous curvature on the membrane is linearly proportional to the density of PS.

To capture the dynamics of [PS] on the outer leaflet, we include (a) diffusion of PS on the membrane surface, (b) curvature-driven feedback of effective PS aggregation and domain formation of the membrane, and (c) the kinetics of the two enzymes TMEM16F and P4ATPases. Thus, we model the time-dependent behavior of [PS] in terms of the area fraction η on the surface of the membrane as follows.

$$\begin{aligned} &\eta_t + \underbrace{\nabla\cdot(\mathbf{v}\eta)}_{\text{advection}} \\ &= \underbrace{k_{\text{scramblase}}\mathrm{e}^{\alpha H(s)}\eta^2(1-\eta)}_{\text{scramblase activity}} - \underbrace{k_{\text{P4ATPase}}\eta\mathrm{e}^{\beta H(s)}}_{\text{P4ATPase activity}} \\ &+ \underbrace{\frac{1}{F_{\text{D}}}\Delta\eta\left[\frac{k_{\text{B}}T}{1-\eta} + 2\kappa\ell^2[\text{PS}]_{\text{sat}}\eta - \gamma\eta\right]}_{\text{diffusion}} - \underbrace{\frac{1}{F_{\text{D}}}\eta\left[\frac{\gamma}{2[\text{PS}]_{\text{sat}}}\Delta^2\eta\right]}_{\text{aggregation}} \\ &- \underbrace{\frac{1}{F_{\text{D}}}2\eta\kappa\ell\Delta H + \frac{1}{F_{\text{D}}}\nabla\eta\cdot\left[\nabla\eta\left(\frac{k_{\text{B}}T}{(1-\eta)^2} + 2\kappa\ell^2[\text{PS}]_{\text{sat}} - \gamma\right)\right.}_{\text{nonlinear interactions}} \\ &\underbrace{\left. - 2\kappa\ell\nabla H - \frac{\gamma}{2[\text{PS}]_{\text{sat}}}\nabla(\Delta\eta)\right]}_{\text{nonlinear interactions}}. \end{aligned} \tag{4}$$

The first term accounts for an increase in PS on the outer leaflet due to the activity of the scramblase, where $k_{\text{scramblase}}$ has units of s^{-1}, since η is dimensionless. The second term accounts for a first-order flipping of PS from the outer leaflet to the inner leaflet due to the P4ATPase activity and k_{P4ATPase} has units of s^{-1}. In both these terms, $H(s)$ is the mean curvature along the arclength s, and α and β, with units of length, are effectively modulating the kinetic parameters based on the local curvature. When both α and β are identically zero, the curvature-mediated feedback is zero in the model. As we will show later, the curvature-driven feedback has a small effect in our model (Fig. S1). The other terms arise from consideration of diffusion of PS on the surface, aggregation due to lipid–lipid interactions, and the resulting nonlinear interaction terms and F_{D} represents the hydrodynamic drag (see supplement and ref. 40 for a complete derivation). While the exact rates of the scramblases and P4ATPases are not known, as we will show later, we obtain these rate constants by fitting to experimental data.

Model summary

Thus, our model captures the key mechanical elements involved in the formation of MPs by balancing the force exerted by the linkers that tether the membrane to the cortex and the opposing membrane deformation driven by applied forces and spontaneous curvature. We simulate the formation of MPs in two scenarios: using linear deformation models, we calculate the conditions that allow for PS aggregation, membrane bending, and linker unbinding using the full system of governing equations (eqn (S18)–(S20)). Once a PS-domain is established, we switch to axisymmetric equations assuming that PS density is localized on the area of the MP bud region and focus on spherical MP formation (Fig. 4). Time dependence enters the model through the rate equation for the linkers and the rate equation for PS kinetics. Thus, while the membrane itself is at mechanical equilibrium, the kinetics of linker binding–unbinding and rate of PS flipping will determine the temporal dynamics of MP formation. All model parameters (Tables S1 and S2), detailed derivations, and numerical schemes are given in the SI.

Results

We analyzed the formation of MPs in response to different biophysical drivers using our model. Even though the individual elements of our model have been analyzed previously, we study the coupled nonlinear system and focus on the formation of highly curved structures and the interplay between the kinetics of PS flipping and the kinetics of adhesive linkers. To our knowledge, previous studies have not studied the combined elements in a nonlinear regime and our analysis provides new insights into how cortical linkage and PS flipping may interact to form MPs.

Linker detachment is required for membrane deformation in response to an instantaneous load

We began by investigating how the membrane-linker combination responds to a point load in the absence of any PS-induced

spontaneous curvature. To do this, we conducted separate simulations of membrane bending due to an applied point load in an axisymmetric configuration. The physical picture is as follows: when an external force (either a point load or a bulk pressure) is applied to the membrane such that the length of the linker springs increases beyond a threshold value (25 nm), the linkers unbind and the membrane detaches from the cortex (Fig. 2A, schematic). To understand this behavior, we first focus on the fraction of bound linkers, ϕ_{lin}, in the absence of membrane bending. From eqn (2) we obtain that the steady state value of ϕ_{lin}, in the absence of membrane bending is given by

$$\phi_{\text{eq}} = \frac{e^{\frac{-\hat{F}\delta}{k_B T}}}{\zeta + e^{\frac{-\hat{F}\delta}{k_B T}}}, \tag{5}$$

where $\zeta = k_{\text{off}}^0/k_{\text{on}}$ and represents the ratio of the two time constants. For ezrin, the characteristic association time on the membrane was measured to be approximately 6.6 s and the characteristic dissociation time was measured to be 5 s,[68] suggesting that ζ is close to 1. Other experiments note that the dissociation constant of ezrin to PIP2 containing vesicles to be approximately 5 μM[69–71] but the individual rate constants are not available. To investigate how ϕ_{eq} changes with membrane bending, we systematically varied the value of ζ in our simulations to account for variations in linker proteins and lipid composition along with an applied load on the membrane.

We first asked whether the relationship between an applied force and membrane bending depends on the linker binding and unbinding time scales. In other words, when coupled with membrane bending, how does the relationship shown in eqn (5) To answer this question, we simulated the deformation of the membrane in response to three different point loads (0.5, 1, and 2 pN) for different values of ζ (Fig. 2A and B). The force required to form a tube for a bare membrane is 2.6 pN[72] and we chose values of forces smaller than these to focus on the membrane deformation. We observed that as the membrane deformed, the regions of high z had zero linkers while the flat regions of the membrane had high density of linkers (Fig. 2B), as expected. We also noted that the final shape of the membrane, for the same fixed force, depended on the value of ζ (Fig. 2A). When ζ was decreased so that the unbinding rate was slower than the binding rate, the linkers took longer to unbind and the bending of the membrane was reduced because the adhesion of the linkers resists the deformation of the membrane (Fig. 2A). The linker detachment kinetics at the center of the membrane depends both on the values of ζ and f_{pull}. At lower values of the pulling force, the membrane deformation is small and complete linker detachment is not observed (Fig. 2B). The coupling between linker binding–unbinding and membrane bending

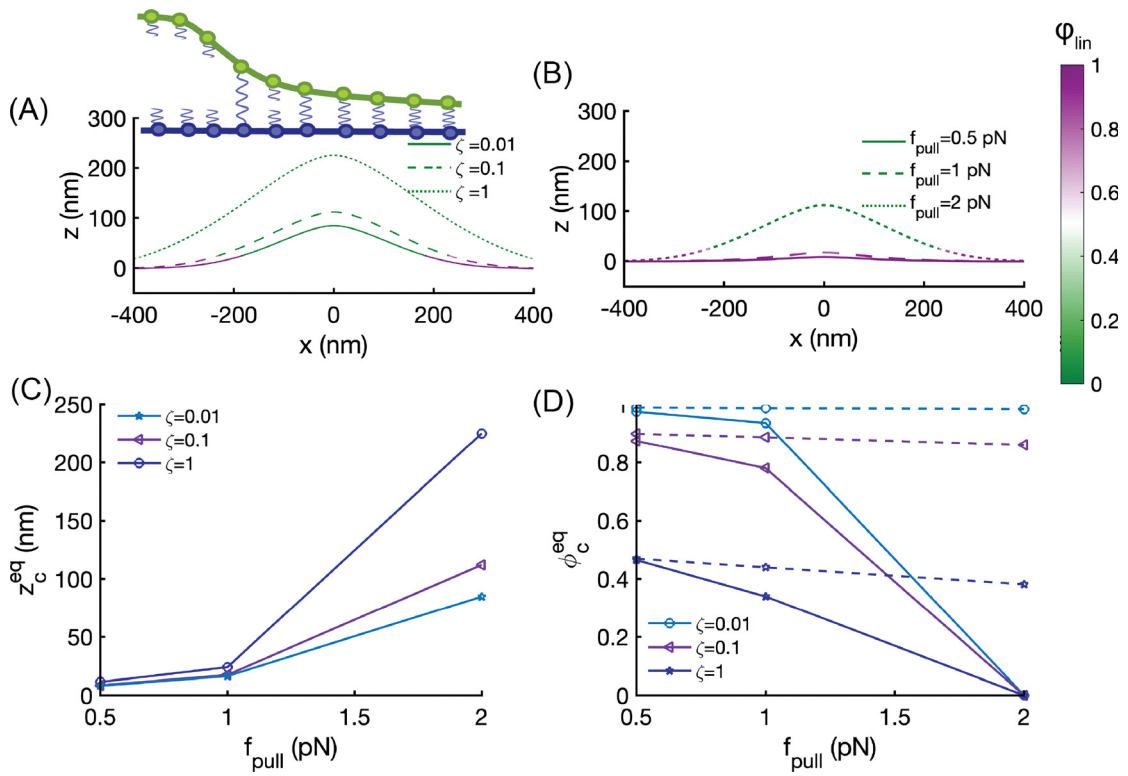

Fig. 2 Competition between linker binding and pulling force determines membrane curvature. (A) Membrane shapes in response to f_{pull} = 2 pN for three different values of $\zeta = k_{\text{off}}^0/k_{\text{on}}$, and (B) membrane shape for ζ = 0.1 and three values of forces f_{pull}. The values of ζ and f_{pull} are shown in the respective panels. (C) Height of the membrane at the center, z_c, as a function of the applied force for three different values of ζ. (D) Comparison between theoretical estimation given in eqn (5) (dashed-line) and numerical findings (solid-line) of the fraction of bound linkers at the center of the membrane as a function of the applied force for three different values of ζ. In all these simulations, the bending modulus was $\kappa = 20k_BT$, tension was λ = 0.001 pN nm^{-1}, and the linker stiffness was k_{lin} = 0.5 pN nm^{-1}.

affects both the height at the center of the membrane (Fig. 2C) and ϕ_{eq} (Fig. 2D). The value of ϕ_{eq} calculated by eqn (5) is shown using dashed lines in Fig. 2D for different values of ζ. We see that the coupling between membrane bending and linker detachment causes significant deviation of ϕ_{eq} at the center of the membrane for different pulling forces. For all values of ζ tested in our simulations, the increase in pulling force causes a greater decrease in ϕ_{eq} at the center of the membrane in the presence of membrane bending compared to the analytical expression in eqn (2), which does not consider membrane bending (Fig. 2D). Thus, our analyses demonstrate that linker detachment is required for membrane bending, and that the timescales of linker binding and unbinding regulate the mechanical response of the membrane to the instantaneous application of a point load. This is consistent with the experimental observations in ref. 29 and 30. Thus, the coupling between membrane bending due to a point load and linker kinetics alters the membrane bending landscape.

Interplay between PS kinetics, curvature generation, and membrane bending

We next investigated how PS diffusion, aggregation, and membrane bending couple with linker detachment. While previous studies have focused on linker detachment for small deformations of the membrane or while ignoring membrane bending,[34] we aimed to study the coupling between membrane bending and linker kinetics in the fully nonlinear regime using Monge parametrization. Using the governing equations (eqn (S18)–(S20)), we simulated the conditions that would lead to the formation of PS domains (Fig. 3). We fixed values of all the model parameters as shown in Table S3. As noted previously,[40] for certain values of lipid-induced spontaneous curvature and aggregation strength, we observe the formation of stable PS domains on the membrane over time (Fig. 3A). Because of the intrinsic coupling between curvature generation and membrane bending, regions of high PS aggregation lead to membrane curvature generation as evidenced by the change in the height of the membrane. Corresponding to the change in the height of the membrane, the density of linkers evolves according to eqn (3) (Fig. 3B). Because the deformation is less than the cutoff distance for the linker, we observed a reduction in linker density but not complete depletion. Finally, because of the coupling between in-plane flow, diffusion, and aggregation of PS, we noted that membrane tension decreases in regions of high PS aggregation (Fig. 3C) consistent with previous works.[38,40] These simulations

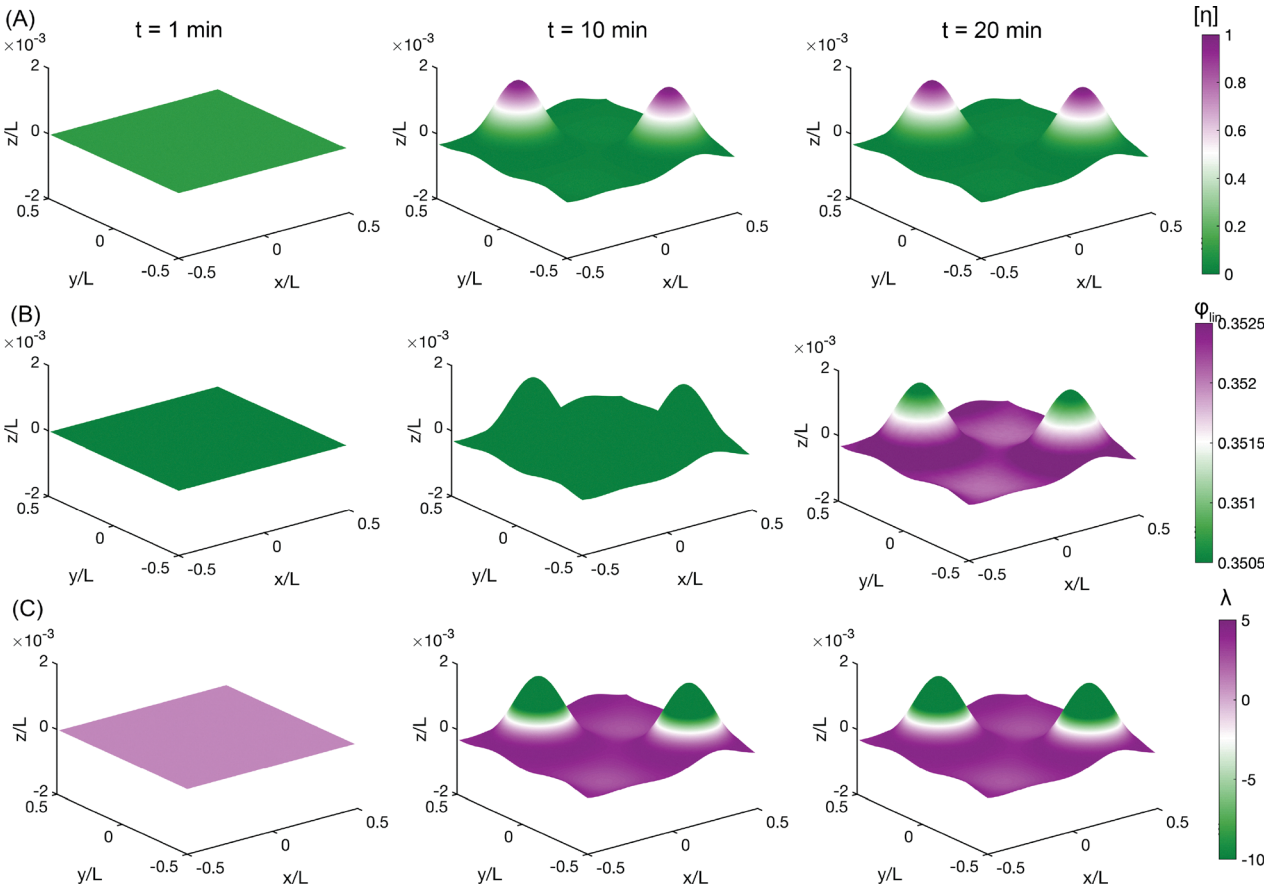

Fig. 3 Coupling between PS aggregation, linker density, and membrane tension for small deformations. (A) Aggregation of PS density over time, density distribution is shown for three time instances on deformed membranes (1 minute, 10 minutes, and 20 minutes). Corresponding density distributions of linkers protein (B) and membrane tension (C) are shown for the same time points on the deformed membrane. In this simulation, the following values were used for parameters: linker stiffness k_{lin} = 0.1 pN nm^{-1}, bending modulus $\kappa = 20k_BT$, membrane tension $\lambda_0 = 1 \times 10^{-4}$ pN nm^{-1}, ζ = 1, aggregation parameters $\hat{A}(=\gamma/k_BT)$ = 25, $\hat{S}(=[PS]_{sat}L^2)$ = 200, membrane size L = 1000 nm, and $\ell/L = 8 \times 10^{-4}$.

established that our model can capture the formation of PS domains, that the linker density changes with respect to membrane bending, and that membrane tension decreases in regions of high spontaneous curvature.

Interaction between PS kinetics and linker properties determines successful MP formation

Having established that our model can lead to the formation of aggregated PS-domains in the Monge deformation, we next sought to simulate the formation of spherical vesicles associated with MP formation. From hereon, all our simulations were conducted in an axisymmetric configuration as described in Fig. 4, where all variables are represented with respect to the arc length coordinate s. As noted in Fig. 4A, the domain of PS aggregates is provided as an input to the model. We specified a spontaneous curvature corresponding to the aggregated PS region (Fig. 4B). The linker force acts on the membrane in the negative z-direction. At the membrane center, the linker density is depleted, leading to a reduced force. Moving away from the center, the force increases as the density of non-depleted linkers rises, but it diminishes again further out due to reduced membrane deformation (Fig. 4C).

Next, we set out to constrain the kinetics of PS flipping to the outer leaflet, which is a key step in MP formation, to experimental observations. The kinetics of PS flipping depend on the kinetics of the scramblase and the P4ATPase (eqn (4)). A majority of experiments use Annexin V as a readout for the presence of PS on the outer surface.[73] In order to fit the rate parameters for our model, we used experimental data from ref. 73 because this study focuses primarily on the role of TMEM16F. We fit our model with the data from Fig. 2B of ref. 73 to obtain the rate parameters for the wild type (WT) condition in our model (Fig. 5A). Based on experimental observations of Annexin V staining,[73] we used a time scale of approximately 15–16 min. Using the 'Curve Fitting toolbox in MATLAB we found the two kinetic parameters to be $k_{\text{scramblase}} = 1.4687\ \text{s}^{-1}$ and $k_{\text{P4ATPase}} = 0.1309\ \text{s}^{-1}$. We focused on the 20 min time scale because that is the time scale used in experiments in the literature.[73] From eqn (4), we note that η, which characterizes the density of PS on the outer membrane is dimensionless, therefore we mapped the PS kinetics to a spontaneous curvature value as a function of time as shown in Fig. 5B. We also varied the kinetics of PS-dependent spontaneous curvature to be faster than the WT or slower than the WT to investigate the effect of scramblase dominance and P4ATPase dominance, respectively.[73] Finally, for interpretation of the model outcome, we defined successful MP formation when the membrane shape develops an overhang (a U-shape such that the angle of the tangent at the neck with the horizontal is greater than $\pi/2$; see SI). Since our model is based on a continuum formulation, we do not simulate scission but rather focus on closing of the neck.[74] We simulated three different PS kinetics: the first tuned to mimic WT PS kinetics, and a slow and a fast case to mimic misregulation of PS exchange between the leaflets, without (Fig. 5) and with curvature-coupled feedback (Fig. S1). For each of these cases, we used three different values of ζ to identify how coupling PS kinetics (and the resulting changes in preferred curvature) with linker kinetics impacts successful MP formation and shape.

When the PS kinetics is slow, in the 20 min time frame, we do not see the formation of a neck for the values of ζ used in our model (Fig. 5C and D). Looking at the maximum deformation at the center of the membrane, we note that there is a clear jump in $z_{\max}$ whenever the linkers are detached (25 nm). After

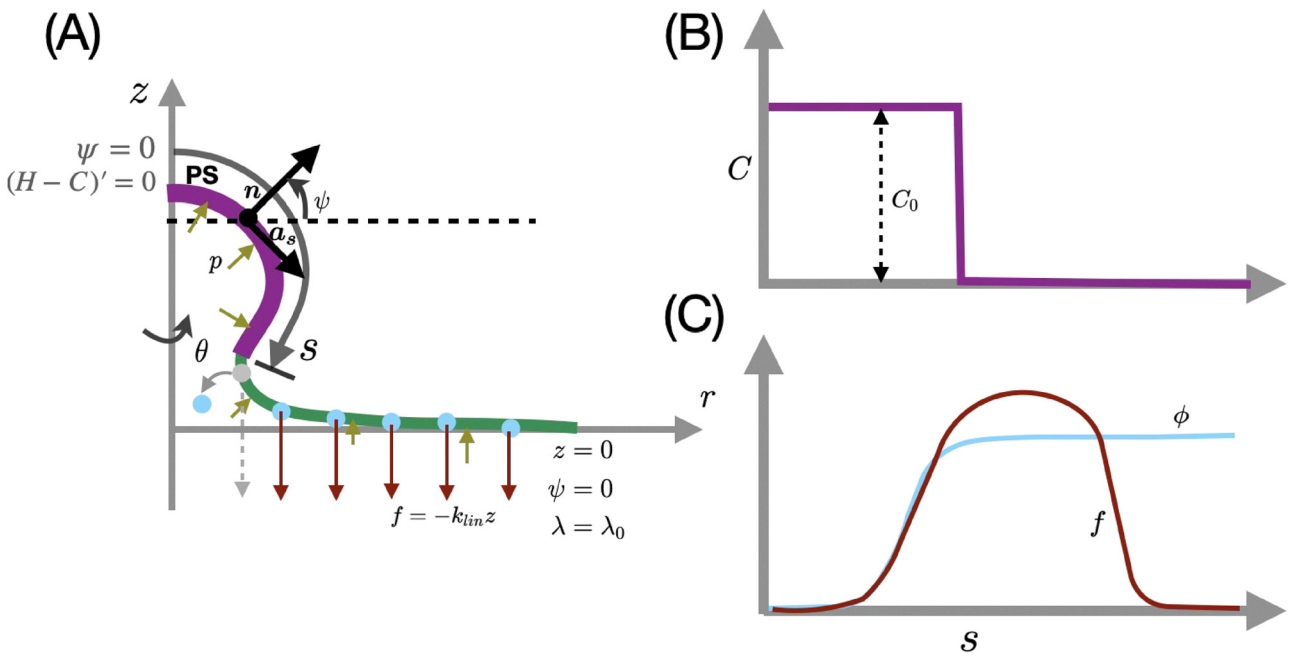

Fig. 4 Schematic of the membrane configuration with input and boundary conditions. (A) Simulation domain of the membrane, distribution of applied force and spontaneous curvature and boundary conditions. (B) Distribution of spontaneous curvature along the arclength, 's' of the membrane. (C) Distribution of linker density and resultant applied force on the membrane along the arclength of the membrane.

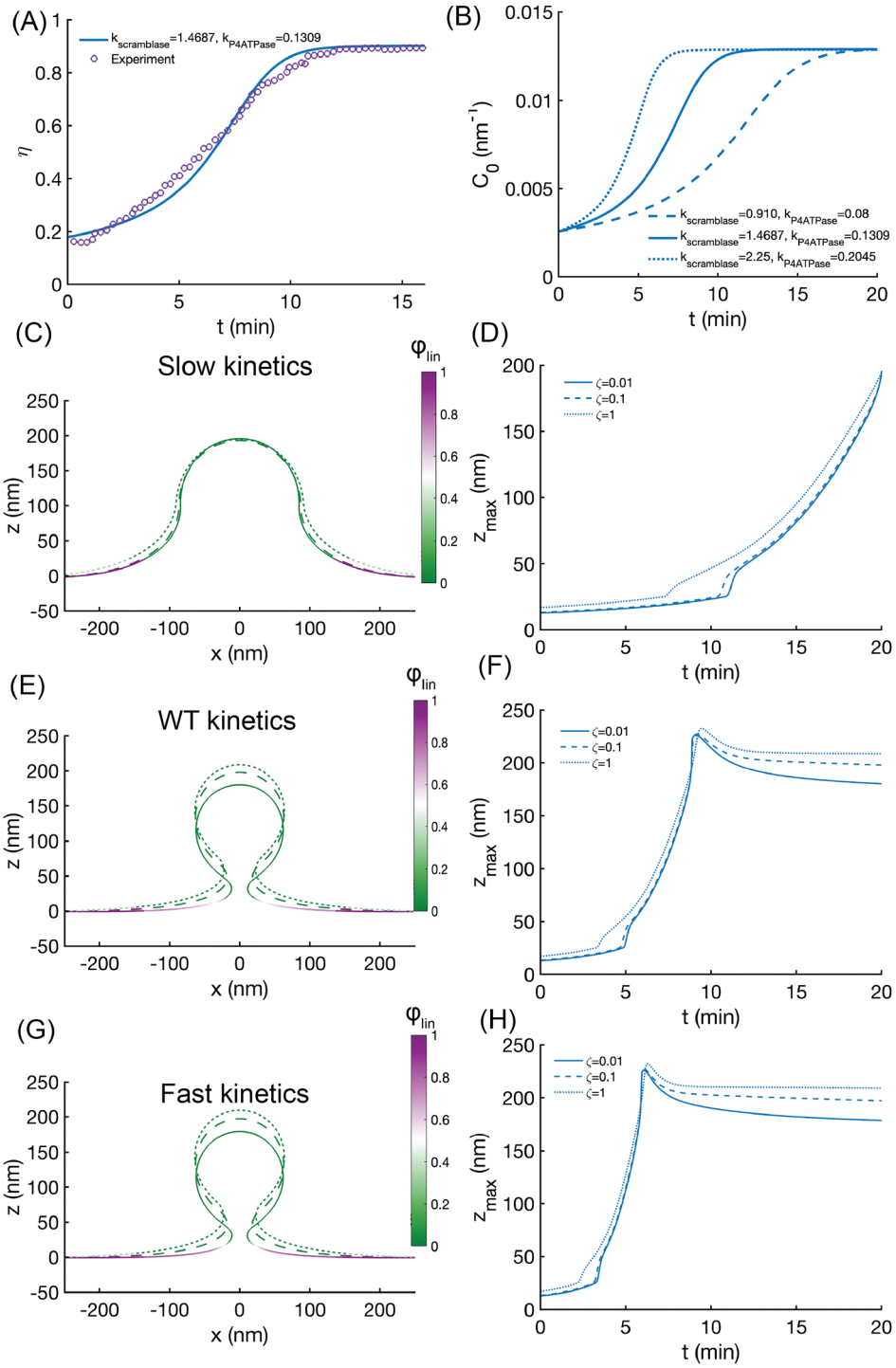

Fig. 5 MP formation depends on PS kinetics (A) PS kinetics in the model were determined by fitting the rate constants in eqn (S11) to experimental data from ref. 73 to obtain a time course for PS kinetics. (B) Spontaneous curvature functions used in our model. WT kinetics (solid line) refers to the time course that matches PS kinetics in panel (A), slow (dashed line) and fast kinetics (dotted line) are obtained by modifying the kinetic parameters in our model as shown in the legend. (C) Membrane shapes for Slow PS kinetics at time 20 minute for three different values of ζ (solid line for ζ = 0.01, dashed line for ζ = 0.1, and dotted line for ζ = 1) and (D) corresponding temporal variation of normal deformation of the membrane. (E) Membrane shapes for WT PS kinetics at time 20 minute for three different values of ζ (ζ = 0.01, ζ = 0.1, ζ = 1) and (F) corresponding temporal variation of normal deformation of the membrane. (G) Membrane shapes for Fast PS kinetics at time 20 minute for three different values of ζ (ζ = 0.01, ζ = 0.1, ζ = 1) and (H) corresponding temporal variation of normal deformation of the membrane. In all these simulations, the bending modulus was $\kappa = 20k_BT$, tension was λ = 0.001 pN nm^{-1}, and spontaneous curvature area was 50 265 nm^2. Linker stiffness was maintained at k_{lin} = 0.5 pN nm^{-1}. The color bar shows the fraction of bound linkers along the membrane stiffness.

this, the deformation is dominated by membrane bending. The time at which the membrane detaches from linkers depends on ζ (Fig. 5D). Using experimentally-constrained WT PS kinetics, without any curvature-coupled feedback (*i.e.* α and β are zero), we noted that for all values of ζ, the shape of the membrane shows a well-formed bud, consistent with the effect of increased PS-induced spontaneous curvature (Fig. 5E). Interestingly, the deformation kinetics revealed the detachment kinetics and snap-through behavior at high z, for all values of ζ, as illustrated in Fig. 5F. In addition to the nonlinearity at early time associated with membrane detachment, we also noted the presence of an additional nonlinearity when the neck forms in the membrane at later times for all values of ζ (Fig. 5F). This transition occurs in two steps: first, the onset of neck formation, where the membrane elongates almost like a thick tube, and second, the reduction of the neck diameter, which occurs simultaneously with spherical deformation, leading to the formation of microparticles. The onset of neck formation is marked by a sudden increase in membrane deformation, followed by a decrease in height as the membrane transforms into a sphere. During this process, the membrane undergoes a snap-through transition, changing from a dome-like to a closed bud-like shape. This snap-through transition is a common phenomenon observed in protein-induced membrane bud formation,[32] protein interactions,[75] and force-mediated tube formation.[72] Similar kinetics, membrane deformation, and snap-through are observed for fast kinetics (Fig. 5G and H). For slow kinetics, we did not observe the snapthrough transition for the neck. In this case, for the chosen values of ζ and spontaneous curvature, the linkers detach in a manner such that the resulting distribution of normal forces is not yet conducive to the formation of a sphere. Across all cases, we noticed that for the same values of PS-induced spontaneous curvature, linker kinetics can determine the final shape of the membrane at a given time. Thus, the feedback between linker kinetics and PS kinetics can determine whether the membrane can form a closed neck that is necessary for scission of the microparticle.

Overall, we find that the onset of bending is thus dependent on the linker forces, and the transition to a well-formed bud is influenced by the spontaneous curvature generated by PS. The nonlinear interactions of these two contributions to membrane bending highlight how the coupling between the linkers and the PS-induced spontaneous curvature can affect the presence of these snap-through instabilities. The temporal evolution of linker density at the center of the membrane as a function of ζ are shown in Fig. S3. The effect of curvature-coupled feedback on the equilibrium shapes of the membrane was minimal, probably due to the simplified model we used (see Fig. S1). However, we observed some deviations in the temporal dynamics of deformation (Fig. S1C) and in the detachments of linkers (Fig. S1D). In all instances, we successfully observed the formation of MP, and overall, the influence of curvature-coupled feedback was quite weak compared to parameters such as linker stiffness. When simulating membrane shapes with faster PS kinetics, we found that while a successful MP can form more quickly (in about 10 minutes) with these kinetics, the crucial detachment and the dependence of the snap-through transition behavior on ζ remain unchanged. In summary, we find that the linkers, through their adhesion force, modify the effective tension on the membrane (eqn (S27)), thus changing the energy landscape of MP formation.

Our results are consistent with experimental observations showing that imbalance of scramblase-flippase activity results in reduced MP formation, which can dampen the procoagulation cascade.[73,76] These results indicate that there exists a balance between the rate of spontaneous curvature induction through PS flipping and linker binding and unbinding. Loss of this balance due to disease states[31,76] can alter mechanics, leading to a failure in MP formation. These simulations predict that the equilibrium shape of the membrane, and therefore successful MP formation, not only depends on the spontaneous curvature induced by the PS, as expected, but also on the interplay between linker lifetimes and the kinetics of PS flipping.

In addition to the binding and unbinding rates, another important linker property is the spring stiffness, k_{lin}. While the exact value of this stiffness is not known, it is possible that the linker crosstalk with the cytoskeleton,[77] and with the

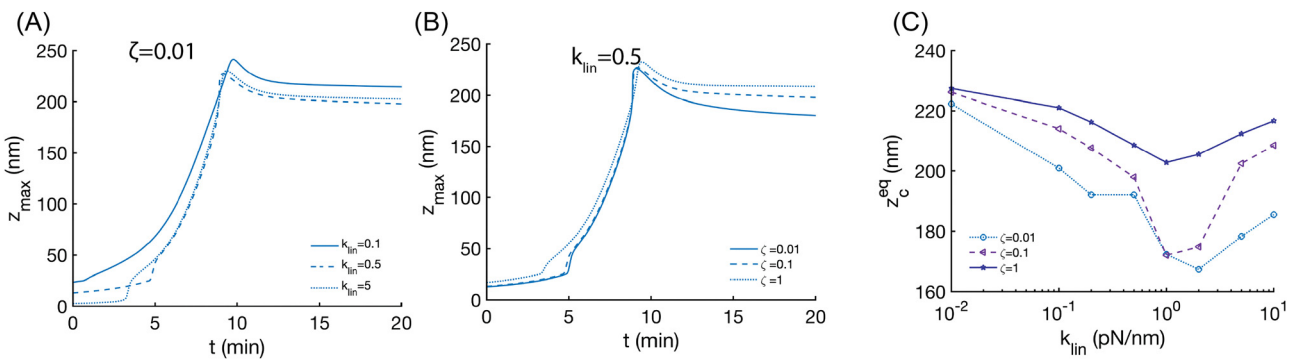

Fig. 6 Linker stiffness determines the effect of PS-induced spontaneous curvature for MP formation. (A) Temporal evolution of height z_{max} at the center of the membrane for ζ = 0.01, WT PS kinetics, and three different values of linker stiffness: k_{lin} = 0.1, 0.5, 5 pN nm^{-1}. (B) Temporal evolution of height z_{max} at the center of the membrane Membrane shape linker stiffness k_{lin} = 0.5, WT PS kinetics, and three different values of ζ (0.01, 0.1, 1). (C) Center height of the membrane at equilibrium as a function for linkers' stiffness k_{lin} for three different values of ζ. In all these simulations, the bending modulus was $\kappa = 20k_BT$, tension was λ = 0.001 pN nm^{-1}, WT PS kinetics were used, and spontaneous curvature area was 50 265 nm^2.

scramblases[31] could lead to altered stiffness.[78] Next, we ask whether the stiffness of the linker could alter the energy landscape of successful MP formation. For all the cases tested, we used the WT PS kinetics and varied ζ and k_{lin} across a range of parameters. For all cases tested, we observed a snapthrough transition (Fig. 6A and B) but the kinetics of maximum deformation at the center depend on the value of k_{lin} and ζ. When we considered the equilibrium deformation at the center of the membrane as a function of k_{lin}, we found a non-monotonic relationship (Fig. 6C). The lowest value of z_c^{eq}, which corresponds to a more well-formed bud, occurs at an intermediate value of k_{lin} for all values of ζ and this effect is pronounced for ζ = 0.01. Thus, our simulations reveal that there exists a complex feedback between linker properties and membrane properties. We observed that the shape of the membrane also depends on the value of the linker stiffness in both cases, highlighting the feedback between membrane mechanics and linker stiffness.

Membrane properties affect MP formation

Finally, we investigated how the properties of the membrane, primarily the bending modulus and the tension, would affect MP formation (Fig. 7). These variations in membrane moduli and tension are designed to capture the biologically observed variations in membrane properties.[79] We used WT PS kinetics and k_{lin} = 0.1 pN nm^{-1} based on the results shown in Fig. 5 and 6. We observed that lower membrane modulus was favorable for MP formation and increasing bending stiffness led to wide open

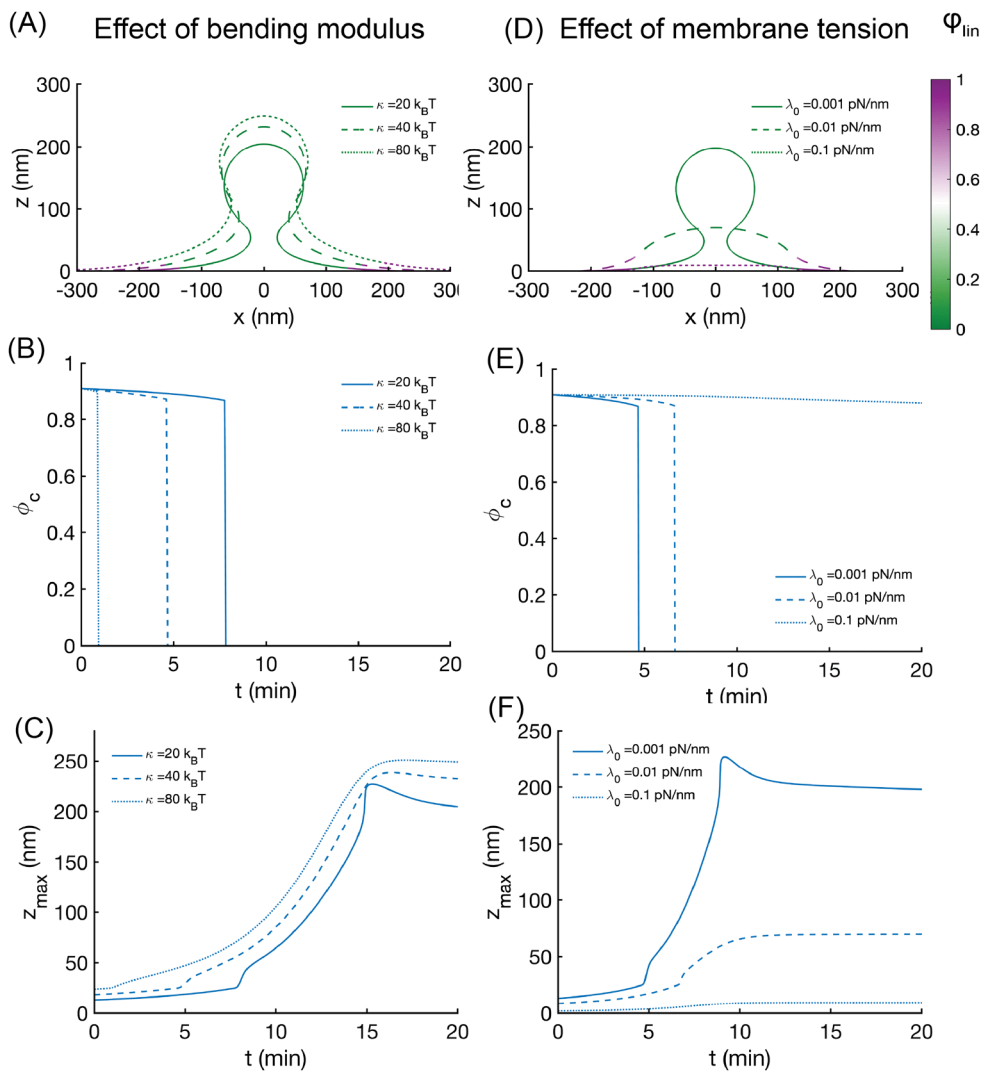

Fig. 7 Combination of membrane parameters aid linker detachment and promote MP formation. (A) Membrane shapes with three different values of bending rigidity for the membrane tension λ_0 = 0.001 pN nm^{-1}. (B) Time evolution of the linker density at the center of the membrane with three different bending rigidities for the membrane tension λ_0 = 0.001 pN nm^{-1}. (C) Time evolution of the height at the center of the membrane with three different bending rigidity for the membrane tension λ_0 = 0.001 pN nm^{-1}. (D) Membrane shapes with three different membrane tensions for bending rigidity κ = 20k_BT. (E) Time evolution of the linkers' density at the center of the membrane with three different membrane tensions for bending rigidity κ = 20k_BT. (F) Time evolution of the height at the center of the membrane with three different membrane tensions for bending rigidity κ = 20k_BT. In all the simulations k_{lin} = 0.5 pN nm^{-1} and WT PS kinetics was used.

necks (Fig. 7A). Furthermore, as the bending modulus increases, linkers detach more rapidly at the center of the membrane, emphasizing the interaction between membrane properties and linker detachment, as shown in Fig. 7B for the same PS kinetics. Fig. 7C illustrates the temporal dynamics of the height at the center of the membrane, revealing that the snap-through transition occurs only for the low bending modulus $\kappa = 20k_BT$ during spherical bud formation.

Similarly, increasing membrane tension leads to a resistance of membrane deformation (Fig. 7D). Since the membrane resists deformation at high tension, the linkers remain attached for longer time (Fig. 7E), and the membrane deformation is smaller (Fig. 7F). Lower membrane tension promotes MP formation, where linker depletion occurs quickly, resulting in a tension distribution across the membrane favorable for a well-formed spherical shape occurs through a snap-through transition during MP formation at a lower tension of 0.001 pN nm^{-1}.

Discussion

Curvature generation in cell membranes is an important biophysical phenomenon that can be explained well by mechanical arguments.[32,33,80,81] In this study, we focused on the formation of MPs as an example to study how outward buds can be generated from the plasma membrane. In order to bend outwards due to spontaneous curvature or externally applied requires membrane detachment from the cortex.[29,30] Our model predicts that the strength of membrane-cortex attachment (regulated by the stiffness and kinetics of linkers) determines the success of MP formation and bleb protrusion. Further, the interplay between linker binding and PS-induced spontaneous curvature suggests some design principles for MP formation: very strong or very weak linkers are not conducive to membrane-cortex detachment; slow kinetics of PS-induced spontaneous curvature are not conducive to MP formation. A balance between membrane-cortex linkers and membrane curvature is essential for the formation of MPs. Many factors can disrupt this balance in the case of disease states, chemoresistance, and drug treatments, and our models suggest ways in which opposing factors can be combined to promote or mitigate MP formation, depending on the pathological state (Fig. 8).

Our model focuses on coupling the mechanics of membrane deformation with linker attachment and PS kinetics. However, this study has not taken into account changes in cytosolic fluidity, coupling with calcium signaling, and associated cytoskeletal remodeling. These simplifications of the underlying cell biology enable computational simplicity, but including these processes is an important aspect of tying the mechanistic aspects of MP formation to biophysical models, and will be a focus of future studies. Despite these simplifications, this model reveals that when kinetics and mechanics are taken into account, surprising nonlinear interactions impact MP formation and bleb expansion. These insights form a theoretical basis for robust experimental investigation into the fundamental mechanisms regulating cell membrane deformation.

A major conclusion from our model is that we need to consider crosstalk between adhesive linkers and the membrane in MP formation. These findings are consistent with experiments that show that ezrin is not present in an expanding bleb[50] and that linker detachment is necessary for membrane protrusions.[30] Based on our predictions, modulating the linker properties should then modify the propensity to form blebs. Charras and colleagues[50] showed that mutant forms of ezrin

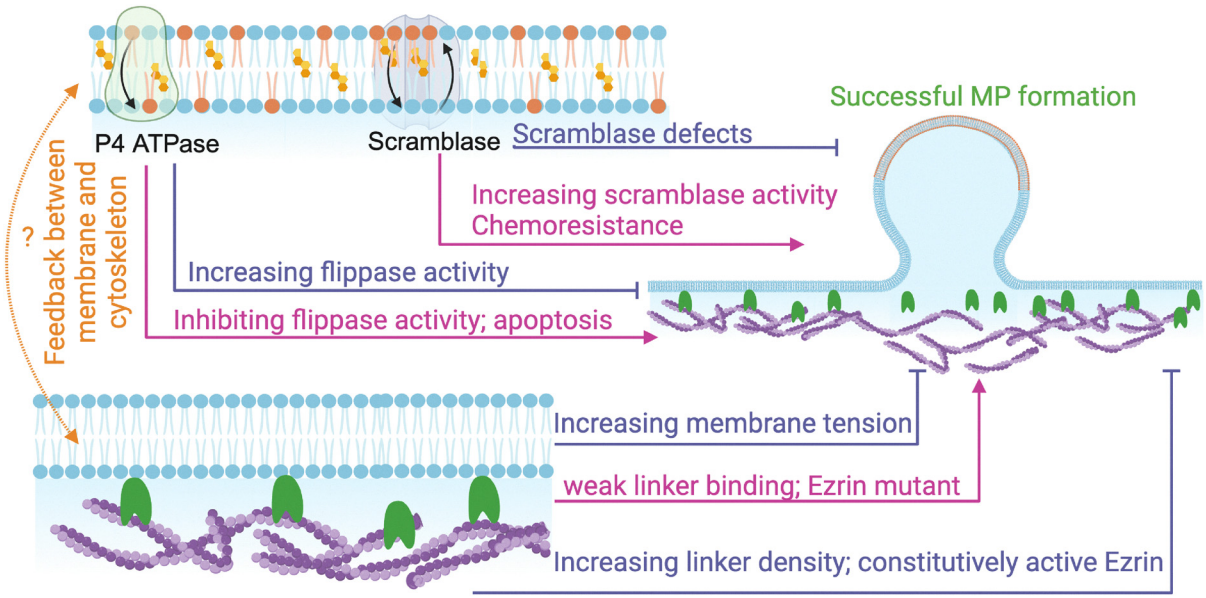

Fig. 8 Interplay between linker properties and lipid properties determines appropriate MP formation. Successful MP formation is a balance of lipid properties and linker strength. Loss of this balance through disease states and drug-induced states can lead to the overproduction or underproduction of MPs. The schematic summarizes a few scenarios that could play a role and outlines the need to explore feedback between the different biophysical players to further shed light into this critical membrane budding phenomenon.

modulate the attachment of the plasma membrane to the cortex. Constitutively active ezrin, which can be expressed as strong binding (low ζ) leads to loss of blebbing, while expressing only the FERM domain weakens the membrane-cortex attachment (see Fig. 8 of ref. 50).

The other major finding from our model is that the rate of spontaneous curvature generation induced by PS flipping kinetics can play an important role in determining the crosstalk between linker detachment and membrane curvature generation. The dependence of MP formation on PS flipping is relevant to Scott syndrome,[76] which is a disease characterized by decreased MP formation (and a resulting decrease in procoagulant activity) due to an inherited defect in lipid scramblase activity.[73,76,82] Studies of the lipid scramblase of the TMEM family have shown that in addition to lipid scrambling, these calcium-activated ion channels interact stoichiometrically with the ezrin–radixin–moesin network[31] and can be negatively regulated by the cytoskeleton.[55] While our model simplifies the PS-induced spontaneous curvature to a kinetic equation, we were able to show that slow PS kinetics (scramblase defect) and fast PS kinetics (constitutively active scramblase) play a role in MP formation. Our findings also have implications for understanding the mechanisms of chemoresistance. In cancer cells, MPs shed from the cell membrane are used to efflux the drug out of the cancer cells. It has been suggested that inhibition of externalization of PS using bisindolylmaleimide-I and D-pantethine, could be used in conjunction with chemotherapy.[83] Thus, future iterations of our modeling approach can have implications for different pathological conditions associated with MP formation.

Author contributions

SAM and PR conceptualized the project scope and designed the simulations, AM derived the continuum description and conducted simulations. All authors co-wrote the manuscript. Funding was obtained by PR.

Conflicts of interest

P. R. is a consultant for Simula Research Laboratories in Oslo, Norway and receives income. The terms of this arrangement have been reviewed and approved by the University of California, San Diego in accordance with its conflict-of-interest policies.

Data availability

Our code is saved at the github repository and can be accessed through this https://github.com/armahapa/Microparticle_formationlink.

Supplementary information (SI): This file contains the detailed derivations of the governing equations, numerical methods used for the simulations, tables of parameters, and supplementary figures. See DOI: https://doi.org/10.1039/d5sm01237f.

Acknowledgements

We thank the members of the Rangamani lab for their feedback and Profs. Itay Budin (UCSD) and Jeanne Stachowiak (UT Austin) for extensive discussions. This project was supported by Office of Naval Research N00014-20-1-2469 and NIGMS R35GM158446 to P. R. S. A. M was also supported by CTMR: P30AR074990.

References

1 L. A. Hargett and N. N. Bauer, *Pulm. Circ.*, 2013, **3**, 329–340.
2 K. D. Brett, N. Z. Nugent, N. K. Fraser, V. M. Bhopale, M. Yang and S. R. Thom, *Sci. Rep.*, 2019, **9**, 13320.
3 K. Segawa, J. Suzuki and S. Nagata, *Proc. Natl. Acad. Sci. U. S. A.*, 2011, **108**, 19246–19251.
4 P. Puddu, G. M. Puddu, E. Cravero, S. Muscari and A. Muscari, *Can. J. Cardiol.*, 2010, **26**, 140–145.
5 J.-M. Freyssinet, *J. Thromb. Haemost.*, 2003, **1**, 1655–1662.
6 J. Auer, *Am. J. Med. Sci.*, 1933, **186**, 776–794.
7 G. L. Kite, *J. Infect. Dis.*, 1914, 319–330.
8 R. Waitz, *Ann. Med.*, 1936, **40**, 413.
9 D. Allan and R. H. Michell, *Biochem. Soc. Trans.*, 1975, **3**, 751–752.
10 D. Allan, M. M. Billah, J. B. Finean and R. H. Michell, *Nature*, 1976, **261**, 58–60.
11 H. U. Lutz, S.-C. Liu and J. Palek, *J. Cell Biol.*, 1977, **73**, 548–560.
12 M. Westerman and J. B. Porter, *Blood Cells, Mol., Dis.*, 2016, **59**, 134–139.
13 P. Muller, T. Pomorski and A. Herrmann, *Biochem. Biophys. Res. Commun.*, 1994, **199**, 881–887.
14 D. Ruhela, V. M. Bhopale, M. Yang, K. Yu, E. Weintraub, A. Greenblatt and S. R. Thom, *Brain, Behav., Immun.*, 2020, **87**, 465–472.
15 D. Ruhela, V. M. Bhopale, S. Kalakonda and S. R. Thom, *Brain Behav., Immun.: Health*, 2021, **18**, 100398.
16 J. H. W. Distler, D. S. Pisetsky, L. C. Huber, J. R. Kalden, S. Gay and O. Distler, *Arthritis Rheum.*, 2005, **52**, 3337–3348.
17 B. Hugel, M. C. Martínez, C. Kunzelmann and J.-M. Freyssinet, *Physiology*, 2005, **20**, 22–27.
18 E. M. Bevers and P. L. Williamson, *Physiol. Rev.*, 2016, **96**, 605–645.
19 J. M. Pasquet, J. Dachary-Prigent and A. T. Nurden, *Eur. J. Biochem.*, 1996, **239**, 647–654.
20 M. A. Savitskaya, I. I. Zakharov and G. E. Onishchenko, *Biochemistry*, 2022, **87**, 191–206.
21 T. Hirama, R. Das, Y. Yang, C. Ferguson, A. Won, C. M. Yip, J. G. Kay, S. Grinstein, R. G. Parton and G. D. Fairn, *J. Biol. Chem.*, 2017, **292**, 14292–14307.
22 R. J. Clarke, K. R. Hossain and K. Cao, *Biochim. Biophys. Acta, Biomembr.*, 2020, **1862**, 183382.
23 T. Sakuragi and S. Nagata, *Nat. Rev. Mol. Cell Biol.*, 2023, **24**, 576–596.
24 K. Balasubramanian, B. Mirnikjoo and A. J. Schroit, *J. Biol. Chem.*, 2007, **282**, 18357–18364.

25 H. Weber, S. Hühns, F. Lüthen and L. Jonas, *Int. J. Exp. Pathol.*, 2009, **90**, 387–399.
26 V. Randriamboavonjy, J. Isaak, A. Elgheznawy, F. Pistrosch, T. Frömel, X. Yin, K. Badenhoop, H. Heide, M. Mayr and I. Fleming, *Blood*, 2012, **120**, 415–423.
27 J. Gilden and M. F. Krummel, *Cytoskeleton*, 2010, **67**, 477–486.
28 H. Li, J. Yang, T. T. Chu, R. Naidu, L. Lu, R. Chandramohanadas, M. Dao and G. E. Karniadakis, *Biophys. J.*, 2018, **114**, 2014–2023.
29 J. Dai and M. P. Sheetz, *Biophys. J.*, 1999, **77**, 3363–3370.
30 E. S. Welf, C. E. Miles, J. Huh, E. Sapoznik, J. Chi, M. K. Driscoll, T. Isogai, J. Noh, A. D. Weems, T. Pohlkamp, K. Dean, R. Fiolka, A. Mogilner and G. Danuser, *Dev. Cell*, 2020, **55**, 723–736.e8.
31 P. Perez-Cornejo, A. Gokhale, C. Duran, Y. Cui, Q. Xiao, H. C. Hartzell and V. Faundez, *Proc. Natl. Acad. Sci. U. S. A.*, 2012, **109**, 10376–10381.
32 J. E. Hassinger, G. Oster, D. G. Drubin and P. Rangamani, *Proc. Natl. Acad. Sci. U. S. A.*, 2017, **114**, E1118–E1127.
33 W. Helfrich, *Z. Naturforsch., C*, 1973, **28**, 693–703.
34 R. Alert, J. Casademunt, J. Brugués and P. Sens, *Biophys. J.*, 2015, **108**, 1878–1886.
35 W. Strychalski and R. D. Guy, *Math. Med. Biol.*, 2012, **30**, 115–130.
36 W. Strychalski and R. D. Guy, *Biophys. J.*, 2016, **110**, 1168–1179.
37 P. Rangamani, A. Agrawal, K. K. Mandadapu, G. Oster and D. J. Steigmann, *Biomech. Model. Mechanobiol.*, 2013, **12**, 833–845.
38 P. Rangamani, K. K. Mandadap and G. Oster, *Biophys. J.*, 2014, **107**, 751–762.
39 D. J. Steigmann, *Arch. Ration. Mech. Anal.*, 1999, **150**, 127–152.
40 A. Mahapatra, D. Saintillan and P. Rangamani, *Soft Matter*, 2021, **17**, 8373–8386.
41 T. Hirama, S. M. Lu, J. G. Kay, M. Maekawa, M. M. Kozlov, S. Grinstein and G. D. Fairn, *Nat. Commun.*, 2017, **8**, 1–14.
42 P. Rangamani, *Biochim. Biophys. Acta, Biomembr.*, 2022, **1864**, 183897.
43 H.-Y. Kim, B. X. Huang and A. A. Spector, *Prog. Lipid Res.*, 2014, **56**, 1–18.
44 N. Wu, H. Song and A. Veillette, *Cell. Mol. Immunol.*, 2021, **18**, 686–697.
45 Y. E. Li, D. M. Norris, F. N. Xiao, E. Pandzic, R. M. Whan, S. Fok, M. Zhou, G. Du, Y. Liu, X. Du and H. Yang, *J. Cell Biol.*, 2024, **223**, e202307041.
46 J. McDonough, T. A. Paratore, H. M. Ketelhohn, B. C. DeCilio, A. H. Ross and A. Gericke, *Membranes*, 2024, **14**, 181.
47 E. Leikina, A. K. Tsaturyan, K. Melikov, J. M. Whitlock, J. Cunanan, M. Roegner, G. Katz, M. M. Kozlov and L. V. Chernomordik, *J. Cell Biol.*, 2025, **225**, e202508055.
48 W. Wang, S. Wu, Z. Cen, Y. Zhang, Y. Chen, Y. Huang, A. R. Cillo, J. S. Prokopec, G. Quarato and D. A. Vignali, *et al.*, *Cell Rep.*, 2022, **41**, 111582.
49 A. Booth, C. J. Marklew, B. Ciani and P. A. Beales, *Faraday Discuss.*, 2021, **232**, 188–202.
50 G. T. Charras, C.-K. Hu, M. Coughlin and T. J. Mitchison, *J. Cell Biol.*, 2006, **175**, 477–490.
51 P. Sens, *Proc. Natl. Acad. Sci. U. S. A.*, 2020, **117**, 24670–24678.
52 K. Xiao and P. Rangamani, *Phys. Rev. Res.*, 2026, **8**, 013012.
53 G. I. Bell, *Science*, 1978, **200**.
54 S.-Z. Lin, J. Prost and J.-F. Rupprecht, *Phys. Rev. E*, 2024, **109**, 054406.
55 H. Lin, J. Roh, J. H. Woo, S. J. Kim and J. H. Nam, *Biochem. Biophys. Res. Commun.*, 2018, **503**, 2348–2354.
56 F.-C. Tsai, A. Bertin, H. Bousquet, J. Manzi, Y. Senju, M.-C. Tsai, L. Picas, S. Miserey-Lenkei, P. Lappalainen, E. Lemichez, E. Coudrier and P. Bassereau, *eLife*, 2018, **7**, e37262.
57 J. M. Phang, S. J. Harrop, A. P. Duff, A. V. Sokolova, B. Crossett, J. C. Walsh, S. A. Beckham, C. D. Nguyen, R. B. Davies, C. Glöckner, E. H. C. Bromley, K. E. Wilk and P. M. G. Curmi, *Biochem. J.*, 2016, **473**, 2763–2782.
58 R. G. Fehon, A. I. McClatchey and A. Bretscher, *Nat. Rev. Mol. Cell Biol.*, 2010, **11**, 276–287.
59 K. P. Hoeflich, S. Tsukita, L. Hicks, C. M. Kay, S. Tsukita and M. Ikura, *Biochemistry*, 2003, **42**, 11634–11641.
60 S. Feng, S. Dang, T. W. Han, W. Ye, P. Jin, T. Cheng, J. Li, Y. N. Jan, L. Y. Jan and Y. Cheng, *Cell Rep.*, 2019, **28**, 567–579.e4.
61 M. E. Falzone, Z. Feng, O. E. Alvarenga, Y. Pan, B. Lee, X. Cheng, E. Fortea, S. Scheuring and A. Accardi, *Nat. Commun.*, 2022, **13**, 2604.
62 R. Watanabe, T. Sakuragi, H. Noji and S. Nagata, *Proc. Natl. Acad. Sci. U. S. A.*, 2018, **115**, 3066–3071.
63 F. Tadini-Buoninsegni, S. A. Mikkelsen, L. S. Mogensen, R. S. Molday and J. P. Andersen, *Proc. Natl. Acad. Sci. U. S. A.*, 2019, **116**, 16332–16337.
64 P. Xu, R. D. Baldridge, R. J. Chi, C. G. Burd and T. R. Graham, *J. Cell Biol.*, 2013, **202**, 875–886.
65 Y. Miyata, K. Yamada, S. Nagata and K. Segawa, *J. Biol. Chem.*, 2022, **298**, 102527.
66 P. F. Devaux, A. Herrmann, N. Ohlwein and M. M. Kozlov, *Biochim. Biophys. Acta*, 2008, **1778**, 1591–1600.
67 J. Liu, Y. Sun, D. G. Drubin and G. F. Oster, *PLoS Biol.*, 2009, **7**, e1000204.
68 M. Fritzsche, R. Thorogate and G. Charras, *Biophys. J.*, 2014, **106**, 343–353.
69 Y. Senju and F.-C. Tsai, *Biophys. Rev.*, 2022, **14**, 199–208.
70 O. Maniti, K. Carvalho and C. Picart, *Biochimie*, 2013, **95**, 3–11.
71 G. Blin, E. Margeat, K. Carvalho, C. A. Royer, C. Roy and C. Picart, *Biophys. J.*, 2008, **94**, 1021–1033.
72 I. Derényi, F. Jülicher and J. Prost, *Phys. Rev. Lett.*, 2002, **88**, 238101.
73 J. Suzuki, M. Umeda, P. J. Sims and S. Nagata, *Nature*, 2010, **468**, 834–838.
74 J. Liu, Y. Sun, D. G. Drubin and G. F. Oster, *PLoS Biol.*, 2009, **7**, e1000204.
75 A. Mahapatra and P. Rangamani, *Soft Matter*, 2023.
76 O. Morel, L. Jesel, J.-M. Freyssinet and F. Toti, *Arterioscler., Thromb., Vasc. Biol.*, 2011, **31**, 15–26.
77 E. Korkmazhan and A. R. Dunn, *Sci. Adv.*, 2022, **8**, eabo2779.
78 E. Leikina, A. K. Tsaturyan, K. Melikov, J. M. Whitlock, J. Cunanan, M. Roegner, G. Katz, M. M. Kozlov

and L. V. Chernomordik, *J. Cell Biol.*, 2026, **225**, e202508055.
79 C. Monzel and K. Sengupta, *J. Phys. D: Appl. Phys.*, 2016, **49**, 243002.
80 A. Mahapatra, D. Saintillan and P. Rangamani, *J. Fluid Mech.*, 2020, **905**, A8.
81 S. A. Malingen and P. Rangamani, *J. R. Soc. Interface*, 2022, **19**, 20220448.
82 A. Piccin, W. G. Murphy and O. P. Smith, *Blood Rev.*, 2007, **21**, 157–171.
83 R. Hayatudin, Z. Fong, L. C. Ming, B.-H. Goh, W.-L. Lee and N. Kifli, *Front. Mol. Biosci.*, 2021, **8**, 629874.

